

Probing chromomagnetic and chromoelectric couplings of the top quark using its polarization in pair production at hadron colliders

Sudhansu S. Biswal,^{1,*} Saurabh D. Rindani,^{2,†} and Pankaj Sharma^{3,‡}

¹*Department of Physics, Orissa University of Agriculture and Technology, Bhubaneswar 751003, India*

²*Physical Research Laboratory, Theoretical Physics Division, Navrangpura, Ahmedabad 380 009, India*

³*Korea Institute for Advanced Study, Hoegi-ro 87, Dongdaemun-gu, Seoul 130-722, Korea*

(Received 7 May 2013; published 16 October 2013)

The Tevatron, where the top quark was discovered, and the currently functional Large Hadron Collider (LHC), with copiously produced top pairs, enable a detailed study of top-quark properties. In particular, they can be used to test the couplings of the top quark to gauge bosons. Several extensions of the standard model (SM) can give rise to anomalous couplings of the top quark to gauge bosons, in particular, the gluons. In this work we examine how top-quark polarization, which is predicted to be negligibly small in the SM, can be used to measure chromomagnetic and chromoelectric couplings of the top quark to gluons. We place special emphasis on the use of angular distributions and asymmetries of charged leptons arising from top decay as measures of top polarization and hence of these anomalous couplings. Sensitivities that may be reached at the Tevatron and the LHC are obtained.

DOI: [10.1103/PhysRevD.88.074018](https://doi.org/10.1103/PhysRevD.88.074018)

PACS numbers: 14.65.Ha, 13.88.+e

I. INTRODUCTION

The Tevatron shut down its operations last year after 8.7 fb^{-1} of accumulated data. The first run of the Large Hadron Collider (LHC) with $\sqrt{s} = 7 \text{ TeV}$ was already completed last year. In that run, the LHC achieved 5.1 fb^{-1} of integrated luminosity. This year it has started at $\sqrt{s} = 8 \text{ TeV}$ and has been projected to collect 15 fb^{-1} of data. After completing its run at $\sqrt{s} = 8 \text{ TeV}$, it is expected to start running at $\sqrt{s} = 14 \text{ TeV}$ in 2014. With the standard model (SM) cross section for top-pair production at $\sqrt{s} = 14 \text{ TeV}$ predicted to be around 830 pb , the LHC will provide ample opportunity to study top properties in detail.

The top quark is the heaviest fundamental particle discovered so far with its mass $m_t = 173.2 \pm 0.9 \text{ GeV}$ [1]. Mainly for this reason, it is considered to be a strong player in the determination of the mechanism of electroweak symmetry breaking. The other consequence of its large mass is that its life time is very short and decays rapidly before any nonperturbative QCD effects can force it into a bound state. Thus, its spin information is preserved in terms of the differential distribution of its decay products. So by studying the kinematical distributions of top decay products, it is, in principle, possible to measure top polarization in any top production process.

While already enough information about the top quark is available, which shows consistency with SM expectations, future runs at the LHC will enable more precise determination of its properties. The most recent experimental value of the top-pair production cross section at the

Tevatron by CDF with 4.6 fb^{-1} of data is $\sigma(t\bar{t}) = 7.5 \pm 0.31(\text{stat}) \pm 0.34(\text{syst}) \text{ pb}$ [2] for $m_t = 172.5 \text{ GeV}$ and is consistent with the measurements from DØ [3]. These measurements are in good agreement with the SM prediction of $\sigma(t\bar{t})_{\text{SM}}^{\text{NNLO}} = 7.08^{+0.00+0.36}_{-0.24-0.27} \text{ pb}$ for $m_t = 173 \text{ GeV}$ [4]. The $t\bar{t}$ cross section has also been measured at the LHC, with a value of $161.9 \pm 2.5(\text{stat})^{+5.1}_{-5.0}(\text{syst})$ from CMS for an integrated luminosity of 2.3 fb^{-1} [5], and $186 \pm 13(\text{stat}) \pm 20(\text{syst}) \pm 7(\text{lum})$ from ATLAS [6], for an integrated luminosity of 2.05 fb^{-1} , in agreement with predictions of the SM.

There seem to be hints of new physics from the study of top-pair production at the Tevatron in the forward-backward asymmetry of the top quark beyond the SM. Recent measurements by CDF [7] and DØ [8] give a larger value for the asymmetry than predicted by the SM.

Experiments at the Tevatron and the LHC have also produced results on top spin correlations [9–12]. The LHC also has results on top polarization [13]. These are consistent with expectations from SM. Particularly, top polarization in the SM is predicted to be nearly vanishing at the LHC because the dominant contributions come from strong interactions, and are therefore parity conserving. Thus any deviation from zero would signal physics beyond SM. The errors are however still large, and new physics is not precluded. In these experiments, polarization is determined by studying the decay distribution in the rest frame of the top quark. The reconstruction of the rest frame entails loss of accuracy. As we will see later, direct observation of the decay distributions in the laboratory frame can be used to probe polarization, and hence infer details of the production mechanism of the top. It is to be expected that this method will suffer from less systematic uncertainties.

Top polarization and its usefulness in the study of new physics scenarios has been extensively treated in the

*sudhansu.biswal@gmail.com

†saurabh@prl.res.in

‡pankajs@kias.re.kr

literature (for some recent papers in the context of hadron colliders, see [14–19]). For example, in Ref. [16], it was shown how top polarization could be utilized to probe the Z' couplings in the Little Higgs (LH) Model. In Ref. [17], the authors showed how top polarization may be used to determine the parameters of the two Higgs doublet model (THDM) and minimal supersymmetric extension of standard model (MSSM). The effect of anomalous Wtb couplings on top polarization in single-top production has been studied in Ref. [18]. Probe of CP violation in single-top production using the polarization of top has been discussed in Ref. [19]. Refs. [20] suggest utilizing top polarization as a probe of models for the top forward-backward asymmetry observed at the Tevatron.

In this work, we study top-pair production at the Tevatron and the LHC in the presence of anomalous gluon couplings to a $t\bar{t}$ pair. In particular, we examine the possibility of using top polarization and other kinematical observables constructed from top decay products in the laboratory frame to measure these anomalous couplings. Our main emphasis will be to show how these laboratory-frame observables can be used to constrain the anomalous couplings. However, since these observables arise from top polarization, they would be a measure of top polarization as well. We therefore first discuss how polarization can give a handle on anomalous couplings.

Top chromomagnetic and chromoelectric couplings which we study here could arise in the SM or from new interactions at loop level. While the CP -conserving chromomagnetic coupling can arise in the SM at one-loop [21], the CP -violating chromoelectric coupling can only be generated at 3-loop level in the SM. Chromomagnetic and chromoelectric dipole moments of the top have been calculated at loop level in various new physics models such as MSSM [22], THDM [23], LH model [24] and in models with unparticles [25].

We calculate our observables at the Tevatron and at the LHC with center-of-mass (cm) energies of 7 (LHC7), 8 (LHC8) and 14 TeV (LHC14). We also look at the sensitivities achieved in all these scenarios including statistical uncertainties with integrated luminosities of 8 at the Tevatron, 5 at LHC7, 10 at LHC8 and 10 fb^{-1} for the case of LHC14.

Anomalous ttg couplings have been studied by several authors in the context of top-pair [26–32], top-pair plus jet [33] and single-top production [34] at hadron colliders. In Ref. [35], the author has used spin correlations in top-pair production at hadron colliders to probe chromomagnetic and chromoelectric dipole moments of top quarks. CP violation in top-pair production at hadron colliders including top chromoelectric couplings is studied in [36].

Apart from having a direct effect on top-pair production at hadron colliders, chromomagnetic and chromoelectric dipole couplings can have an indirect effect and modify the decay rate of $b \rightarrow s\gamma$ at loop level [37,38]. Using the

measured branching ratio $\text{Br}(b \rightarrow s\gamma)$ [38], tight bounds on the chromomagnetic dipole coupling ρ were extracted, viz., $0.03 < \rho < 0.01$.

At the Tevatron and at the LHC, the dominant process of top production, viz., top-pair production, takes place through chirality-conserving QCD couplings in the SM. Thus, in the SM, the top polarization in top-pair production can only occur through the electroweak quark-antiquark annihilation into a virtual Z and is negligibly small. Any new physics in which new couplings to top are chiral can increase top polarization. The measurement of top polarization is thus an important tool to study new physics in top-pair production. However, top polarization can only be measured through the distributions of its decay products. Hence, any new physics in top decay may contaminate the measurement of top polarization and, therefore, of the new physics contribution in top production. Assuming only SM particles, any new physics in top decay can be parametrized in terms of anomalous tbW couplings as

$$\Gamma^\mu = \frac{-ig}{\sqrt{2}} V_{tb} \left[\gamma^\mu (f_{1L} P_L + f_{1R} P_R) + \frac{i\sigma^{\mu\nu}}{m_W} (p_t - p_b)_\nu (f_{2L} P_L + f_{2R} P_R) \right], \quad (1)$$

where in SM $f_{1L} = 1$ and $f_{1R} = f_{2L} = f_{2R} = 0$. Under the assumptions that (i) anomalous tbW couplings are small, (ii) the top is on-shell and (iii) $t \rightarrow bW^+$ is the only decay channel, it was shown in Refs. [39] that the charged-lepton angular distributions are independent of the anomalous tbW couplings. Thus, one can say that the charged-lepton angular distributions are clean and uncontaminated probes of top polarization and thus of any new physics responsible for top production.

For the above reasons, we choose, apart from top polarization, an asymmetry constructed out of the azimuthal distribution of charged leptons arising from top decay.

In our work, we concentrate on the leptonic decay state arising from either t or \bar{t} in top-pair production. That is, we look at observables constructed from the charged lepton produced in t (\bar{t}) decay, while the \bar{t} (t) can decay into either a leptonic or a hadronic final state. Often we do not distinguish between observables related to t and those related to \bar{t} . Thus measurements made for the top quark could also be made for the top antiquark in the process of top-pair production, and the results combined. However, in this case, information on CP violation would be lost. For the specific case of measurement of the CP -violating chromoelectric coupling, t and \bar{t} observables have to be treated separately, and the corresponding partial cross sections appropriately added or subtracted.

The rest of the paper is organized as follows. In the next section we discuss the formalism and the framework of our work. In Sec. III we discuss the application of the framework to the process of inclusive top-pair production at the Tevatron and the LHC and present our results for the

observables like top polarization, charged-lepton angular distributions and the lepton azimuthal asymmetry. Section IV deals with the statistical sensitivity of our observables to the anomalous couplings. The following section contains the conclusions. The Appendix lists the production spin density matrix elements at the parton level for gg and $q\bar{q}$ initial states.

II. THE FRAMEWORK

We now describe the formalism underlying our analysis.

We define the top-quark anomalous couplings to gluons including chromomagnetic and chromoelectric dipole form factors by the $t\bar{t}g$ vertex

$$\Gamma^\mu = \frac{g_s}{m_t} \sigma^{\mu\nu} (\rho + i\rho'\gamma_5) q_\nu, \quad (2)$$

where ρ and ρ' are the chromomagnetic and chromoelectric form factors, respectively, q_ν is momentum of the gluon and m_t is the mass of top quark. Of these, the ρ term is CP conserving, whereas the ρ' term is CP violating. We will treat the form factors ρ and ρ' as complex. Moreover, even though these form factors are in principle energy-dependent functions, we will work in the approximation that they are constant. We will therefore often refer to them as ‘‘couplings.’’ In the SM, both ρ and ρ' are zero at tree level.

For the calculation of the final-state charged-lepton distributions arising from either t or \bar{t} , we use the spin density matrix formalism. Since the top width of about 1.5 GeV is small compared to its mass, the narrow-width approximation,

$$\left| \frac{1}{p^2 - m_t^2 + im_t\Gamma_t} \right|^2 \approx \frac{\pi}{m_t\Gamma_t} \delta(p^2 - m_t^2), \quad (3)$$

can be utilized to factor the squared amplitude into production and decay parts as

$$|\overline{\mathcal{M}}|^2 = \frac{\pi\delta(p_t^2 - m_t^2)}{\Gamma_t m_t} \sum_{\lambda, \lambda'} \rho^{\lambda\lambda'} \Gamma^{\lambda\lambda'}, \quad (4)$$

where $\rho^{\lambda\lambda'}$ and $\Gamma^{\lambda\lambda'}$ are, respectively, the 2×2 top production and decay spin density matrices and $\lambda, \lambda' = \pm$ denote the sign of the top helicity. The density matrices may be defined in terms of the spin-dependent amplitudes as follows:

$$\rho^{\lambda\lambda'} = \sum_{\mu} M_{\lambda\mu}^{\text{prod}} M_{\lambda'\mu}^{\text{prod}*}, \quad (5)$$

$$\Gamma^{\lambda\lambda'} = M_{\lambda}^{\text{decay}} M_{\lambda'}^{\text{decay}*}. \quad (6)$$

Here $M_{\lambda\mu}^{\text{prod}}$ is the amplitude for top-pair production, with the sign of top helicity λ , and that of the antitop helicity μ . $M_{\lambda}^{\text{decay}}$ is the amplitude for the decay of the top with

helicity λ . Analogous expressions may be written down for the density matrices for the antitop quark.

After phase space integration of $\rho^{\lambda\lambda'}$, we get the resulting polarization density matrix $\sigma^{\lambda\lambda'}$. The (1,1) and (2,2) diagonal elements of $\sigma^{\lambda\lambda'}$ are the cross sections for the production of positive and negative helicity tops and $\sigma_{\text{tot}} = \sigma^{++} + \sigma^{--}$ is the total cross section.

Using Eq. (4) we can write the partial cross section in the parton cm frame as

$$d\sigma = \frac{1}{32(2\pi)^4 \Gamma_t m_t} \int \left[\sum_{\lambda, \lambda'} \frac{d\sigma^{\lambda\lambda'}}{d\cos\theta_t} \left(\langle \Gamma^{\lambda\lambda'} \rangle \right) \right] \times d\cos\theta_t d\cos\theta_\ell d\phi_\ell E_\ell dE_\ell dp_W^2, \quad (7)$$

where the b -quark energy integral is replaced by an integral over the invariant mass p_W^2 of the W boson, its polar-angle integral is carried out using the Dirac delta function of Eq. (3) and the average over its azimuthal angle is denoted by the angular brackets. We obtain analytical expressions for the spin density matrix for top-pair production including the contributions of anomalous $t\bar{t}g$ couplings to linear order at the parton level. These expressions for gg and $q\bar{q}$ initial states are listed separately in the Appendix. Use has been made of the analytic manipulation program FORM [40]. The expressions for the top-decay spin density matrix has been evaluated without linear approximation in anomalous tbW couplings in Ref. [18]. However, since we plan to work to linear order also in the tbW anomalous couplings, and evaluate observables dependent only on lepton angular variables, we need not include the dependence on tbW anomalous couplings.

III. THE TOP-PAIR PRODUCTION PROCESS

We make use of the analytical expressions for the spin density matrix for $t\bar{t}$ production, including anomalous ttg couplings to linear order listed in the Appendix. QCD gauge invariance of the ttg anomalous couplings requires a $ggtt$ four-point coupling, which has also been included in our expressions. We find that at linear order, the real part of the coupling ρ and the imaginary part of the coupling ρ' give significant contributions to the diagonal elements of production density matrix, which are the ones that contribute to top polarization. The off-diagonal elements of the matrix get contributions from $\text{Im}\rho$ and $\text{Im}\rho'$, but not from the real parts of the anomalous couplings. The parton-level distributions are convoluted with parton distributions, which we do numerically.

We neglect all fermion masses except that of the top and set $V_{tb} = 1$. For numerical calculations, we use the leading-order parton distribution function (PDF) set CTEQ6L [41] with a factorization scale of $m_t = 173.2$ GeV. We also evaluate the strong coupling at the same scale, $\alpha_s(m_t) = 0.1085$. We make use of the following values for other parameters: $M_W = 80.403$ GeV, the electromagnetic coupling $\alpha_{\text{em}}(m_Z) = 1/128$ and $\sin^2\theta_W = 0.23$. We neglect

the electroweak contributions in the production process. We take only one coupling to be nonzero at a time in the analysis except in Sec. IV, where we show how simultaneous limits on two of the anomalous ttg couplings may be obtained. In evaluating the angular distribution of the charged lepton from top decay, we impose the acceptance cuts $p_T^\ell > 20$ GeV and $|\eta| < 2.5$ on the transverse momentum p_T^ℓ and rapidity η of the charged lepton.

A. Top polarization

The degree of longitudinal polarization P_t of the top quark is given by

$$P_t = \frac{\sigma^{++} - \sigma^{--}}{\sigma^{++} + \sigma^{--}}, \quad (8)$$

with an analogous expression for the polarization of the top antiquark.

In the SM, P_t is predicted to be zero at tree level for top-pair production neglecting the contributions of s -channel γ , Z exchange in $q\bar{q}$ annihilation. We find that including nonvanishing anomalous ttg couplings, there can be nonzero top polarization asymmetry. In the expressions for the spin density matrix for top-pair production, we see that the contributions of $\text{Im}\rho'$ have opposite signs in (1, 1) and (2, 2) elements and hence lead to nonzero P_t , while the contributions of $\text{Re}\rho$ have the same sign in these elements and thus do not contribute to top polarization. Thus top polarization can be utilized to measure the coupling $\text{Im}\rho'$ independently of all other anomalous ttg couplings. The diagonal elements of the density matrix for \bar{t} also show that the polarization of \bar{t} is the same as that of t , confirming that $P_t + P_{\bar{t}}$ is indeed a measure of CP violation, proportional to the CP -odd coupling $\text{Im}\rho'$. P_t is shown in Fig. 1 as a function of anomalous coupling $\text{Im}\rho'$ in the linear approximation, for the Tevatron and for the LHC7, LHC8 and LHC14. The grey bands in the figures denote the 3σ statistical uncertainty in the measurement of P_t . The grey band is the thinnest for the 14 TeV LHC because it has the largest cross section and therefore the smallest statistical error.

We also study the effect of top- p_T cut on top polarization. In Fig. 1, we show top polarization for two different values of p_T cut i.e. $p_T > 100$ GeV and $p_T < 100$ GeV. We find that for low- p_T tops, the top polarization is larger compared to high- p_T tops for the LHC while for the Tevatron, this observation is opposite. At Tevatron, high- p_T tops tend to have higher degree of polarization.

We can understand the observation regarding the Tevatron as follows: At the Tevatron, the $q\bar{q}$ contribution dominates. In the diagonal elements of the spin density matrix for the $q\bar{q}$ -initiated contribution shown in the Appendix, the coefficient of $\text{Im}\rho'$ is proportional to $\sin^2\theta_t = (p_T'/p')^2$. It is the $\text{Im}\rho'$ which gives rise to the polarization, and so P_t is proportional to $(p_T')^2$ at the Tevatron, and it increases with transverse momentum. As for the LHC, the result is not so easy to see.

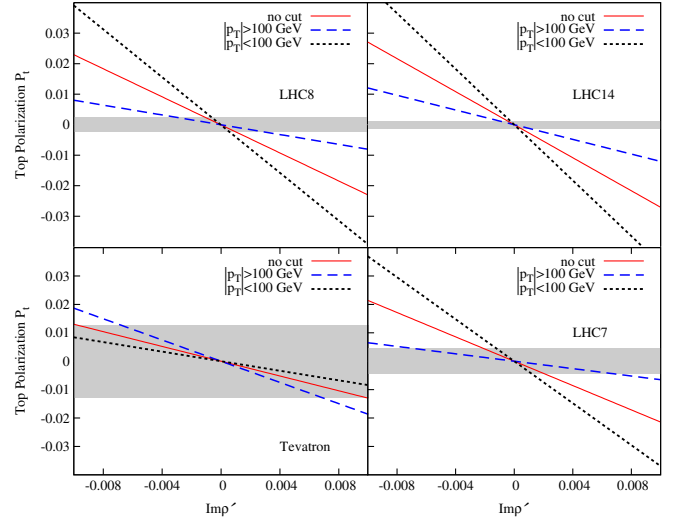


FIG. 1 (color online). The top polarization P_t in $t\bar{t}$ production at the Tevatron (bottom left), LHC7 (bottom right), LHC8 (top left) and LHC14 (top right) as a function of the anomalous ttg coupling $\text{Im}\rho'$. The grey band shows the 3σ error interval in the SM without any p_T cut.

B. Angular distributions of the charged lepton

Top polarization can be determined through the angular distribution of its decay products. In the SM, the dominant decay mode is $t \rightarrow bW^+$, with a branching ratio (BR) of 0.998, with the W^+ subsequently decaying to $\ell^+ \nu_\ell$ (semileptonic decay, BR 1/9 for each lepton) or $u\bar{d}$, $c\bar{s}$ (hadronic decay, BR 2/3). The angular distribution of a decay product f for a top-quark ensemble has the form

$$\frac{1}{\Gamma_f} \frac{d\Gamma_f}{d\cos\theta_f} = \frac{1}{2} (1 + \kappa_f P_t \cos\theta_f). \quad (9)$$

Here θ_f is the angle between fermion f and the top spin vector in the top rest frame and P_t [defined in Eq. (8)] is the degree of polarization of the top-quark ensemble. Γ_f is the partial decay width and κ_f is the spin analyzing power of f . Obviously, a larger κ_f makes f a more sensitive probe of the top spin. The charged lepton and the d quark are the best spin analyzers with $\kappa_{\ell^+} = \kappa_{\bar{d}} = 1$, while $\kappa_{\nu_\ell} = \kappa_u = -0.30$ and $\kappa_b = -\kappa_{W^+} = -0.39$, all κ values being at tree level [42]. Thus the ℓ^+ or d have the largest probability of being emitted in the direction of the top spin and the least probability in the direction opposite to the spin. Since at the LHC, the lepton energy and momentum can be measured with high precision, we focus on leptonic decays of the top.

In this work, we focus on laboratory-frame angular distributions of the charged lepton, which obviate the need for event by event transformation to the rest frame of the top quark as would be needed for measurement of top polarization using (7). Also, as mentioned earlier and shown in Refs. [39], the charged-lepton angular

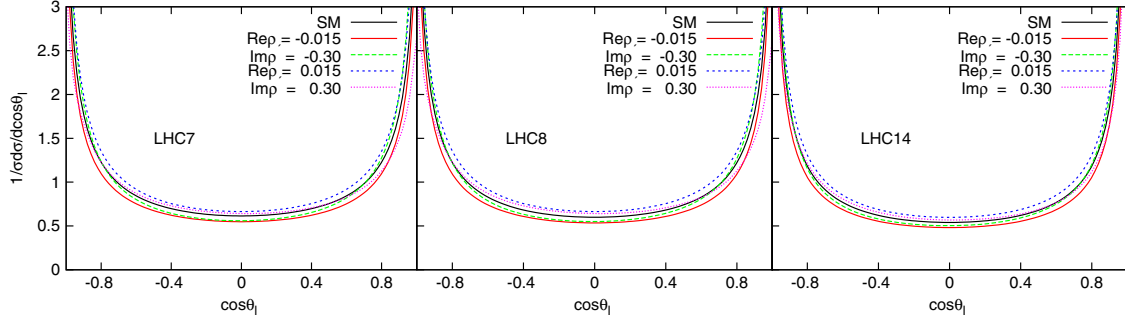


FIG. 2 (color online). The normalized polar-angle distribution of the charged lepton in $t\bar{t}$ production at the LHC7 (left), LHC8 (center) and LHC14 (right) for the SM and with anomalous ttg couplings.

distribution in the lab frame is independent of any new physics in top decay and is thus a clean and uncontaminated probe of new physics in top production.

We first obtain the angular distribution of the charged lepton in the parton cm frame, by integrating over the lepton energy, with limits given by $m_W^2 < 2(p_t \cdot p_\ell) < m_t^2$. This integral can be done analytically, giving the following expression for the differential cross section in the parton cm frame,

$$\begin{aligned} \frac{d\sigma}{d\cos\theta_t d\cos\theta_\ell d\phi_\ell} &= \frac{1}{32\Gamma_t m_t} \frac{1}{(2\pi)^4} \int \left[\sum_{\lambda, \lambda'} \frac{d\sigma^{\lambda\lambda'}}{d\cos\theta_t} g^4 \mathcal{A}^{\lambda\lambda'} \right] |\Delta(p_W^2)|^2 dp_W^2, \end{aligned} \quad (10)$$

where

$$\begin{aligned} \mathcal{A}^{\pm\pm} &= \frac{m_t^6}{24(1 - \beta_t \cos\theta_{t\ell})^3 E_t^2} \\ &\times [(1 - r^2)^2 (1 \pm \cos\theta_{t\ell})(1 \mp \beta_t)(1 + 2r^2)], \end{aligned} \quad (11)$$

$$\begin{aligned} \mathcal{A}^{\pm\mp} &= \frac{m_t^7}{24(1 - \beta_t \cos\theta_{t\ell})^3 E_t^3} \\ &\times \sin\theta_{t\ell} e^{\pm i\phi_\ell} [(1 - r^2)^2 (1 + 2r^2)]. \end{aligned} \quad (12)$$

Here $r = m_W/m_t$ and $\cos\theta_{t\ell}$ is the angle between the top quark and the charged lepton in top decay in the parton cm frame, given by

$$\cos\theta_{t\ell} = \cos\theta_t \cos\theta_\ell + \sin\theta_t \sin\theta_\ell \cos\phi_\ell, \quad (13)$$

where θ_ℓ and ϕ_ℓ are the lepton polar and azimuthal angles.

In the lab frame, we define the lepton polar angle with respect to either beam direction as the z axis and the azimuthal with respect to the top-production plane chosen as the x - z plane, with the convention that the x component of the top momentum is positive. At the LHC, which is a symmetric collider, it is not possible to define a positive sense for the z axis. Hence lepton angular distribution is

symmetric under interchange of θ_ℓ and $\pi - \theta_\ell$ as well as of ϕ_ℓ and $2\pi - \phi_\ell$.

We first look at the polar-angle distribution of the charged lepton and the effect on it of anomalous ttg couplings. As can be seen from Fig. 2, where we plot the polar-angle distribution for LHC7, LHC8 and LHC14, the normalized distributions (here and later, we normalize distributions to the SM cross sections) are insensitive to anomalous ttg couplings. On the other hand, for the Tevatron, the polar-angle distribution are found to be somewhat sensitive as can be seen from Fig. 3. The sensitivity of polar-angle distributions on the anomalous ttg couplings have been studied in detail in Ref. [28] for the Tevatron, LHC7 and LHC14. Our results for these distributions agree with them. It is interesting to note that even though it is possible in principle to have a forward-backward asymmetric distribution at the Tevatron, the chromomagnetic and chromoelectric couplings in Eq. (2) do not generate an asymmetry.

We next look at the contributions of anomalous couplings to the azimuthal distribution of the charged lepton. In Fig. 4 we show the normalized azimuthal distribution of the charged lepton in a linear approximation of the couplings for Tevatron, LHC7, LHC8 and LHC14 for different values of $\text{Re}\rho$ and $\text{Im}\rho'$ taken nonzero one at a

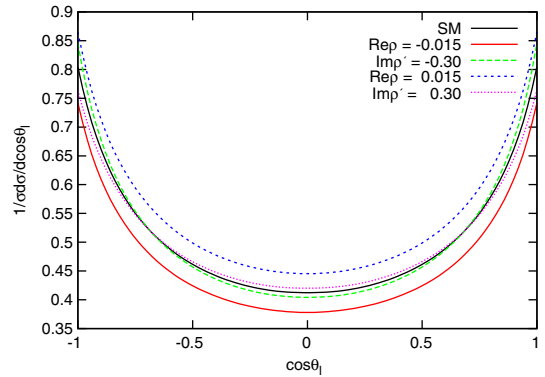


FIG. 3 (color online). The normalized polar-angle distribution of the charged lepton in $t\bar{t}$ production at the Tevatron for the SM and with anomalous ttg couplings.

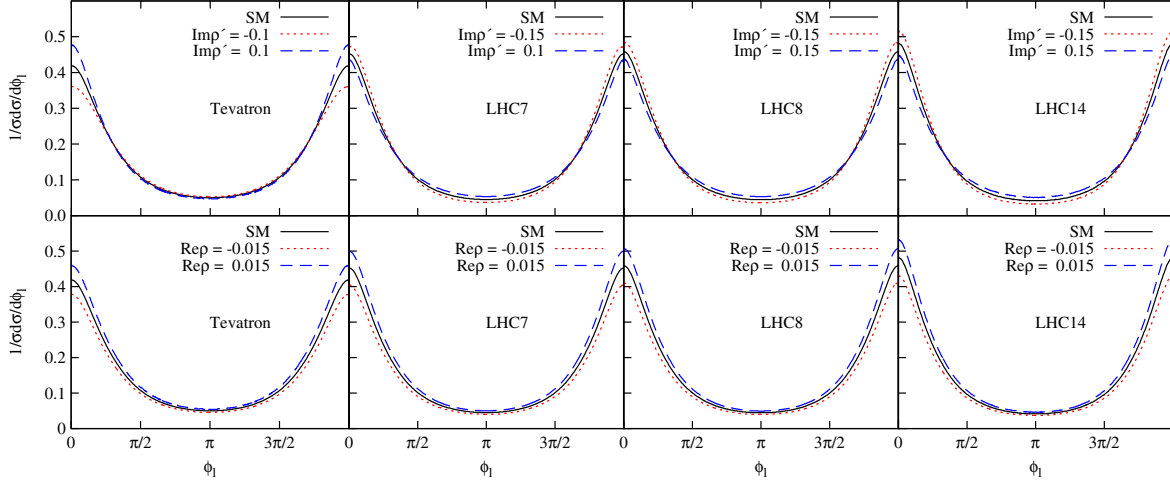


FIG. 4 (color online). The normalized azimuthal distribution of the charged lepton in $t\bar{t}$ production at the Tevatron, LHC7, LHC8 and LHC14 for anomalous ttg coupling $Re\rho$ (bottom) and $Im\rho'$. Also shown in each case is the distribution for the SM.

time. We see that the curves for the couplings $Re\rho$ and $Im\rho'$ peak near $\phi_\ell = 0$ and $\phi_\ell = 2\pi$.

In principle, it is possible to separate the dependence on the two couplings by taking the sum and difference of the distributions for t and \bar{t} . The difference would be CP odd, and hence dependent only on $Im\rho'$, whereas the sum would be CP even, depending only on $Re\rho$.

We now discuss two angular asymmetries which would serve as a measure of the anomalous couplings. The first depends on the polar-angle distributions of the charged leptons from t and \bar{t} , and the second one on the azimuthal distributions.

C. Charge asymmetry

We first look at a CP -violating asymmetry which is generated by the difference in the charged-lepton polar-angle distributions arising from the top and the antitop. We define the charge asymmetry

$$A_{\text{ch}}(\theta_0) = \frac{1}{2\sigma_{\text{SM}}(\theta_0)} \int_{-\cos\theta_0}^{\cos\theta_0} d\cos\theta \left(\frac{d\sigma^+}{d\cos\theta} - \frac{d\sigma^-}{d\cos\theta} \right), \quad (14)$$

where $d\sigma^\pm/d\cos\theta$ denote the differential cross sections for ℓ^+ and ℓ^- production from t and \bar{t} decay, respectively, and $\sigma_{\text{SM}}(\theta_0)$ is the cross section for either ℓ^+ or ℓ^- production, with a cutoff of θ_0 in the forward and backward directions of the lepton. It is obvious that for $\theta_0 = 0$, the numerator of Eq. (14) vanishes, because it measures the difference in the ℓ^+ and ℓ^- production rates at all angles, which is zero from charge conservation. However, with a cutoff θ_0 , $A_{\text{ch}}(\theta_0)$ can be nonzero, and is a measure of CP violation. It can be seen from the equations in the Appendix that $A_{\text{ch}}(\theta_0)$ is proportional to $Im\rho'$.

We plot in Fig. 5 the cross sections for charged leptons ℓ^\pm coming from decay of top/anti-top in top pair production as a function of cutoff angle θ_0 . We see from Fig. 5

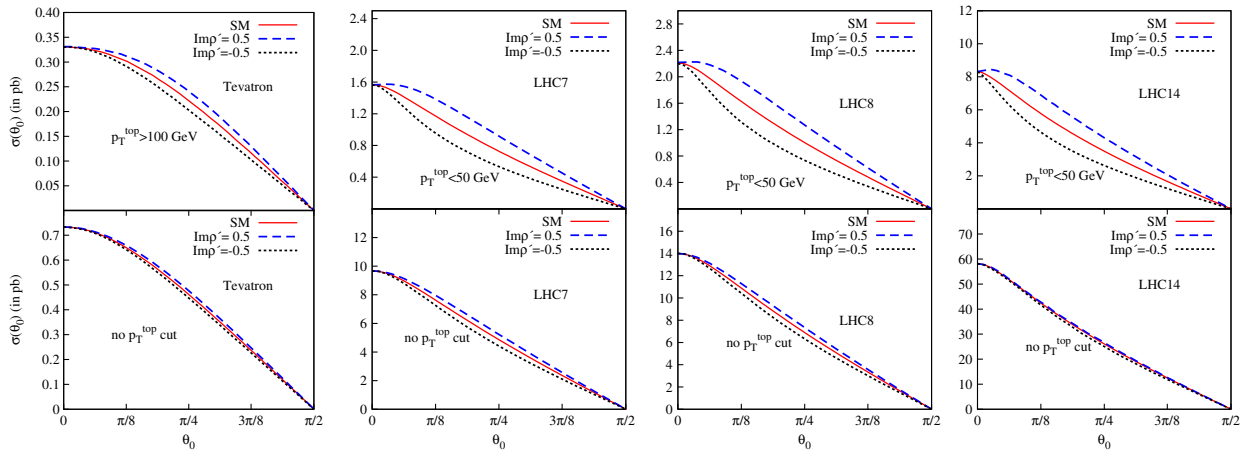


FIG. 5 (color online). The cross section as a function of cutoff angle θ_0 of the charged lepton in top-pair production at the Tevatron (bottom left), LHC7 (bottom right), LHC8 (top left) and LHC14 (top right) for anomalous ttg coupling $Im\rho'$. The SM cross section is also shown in each case.

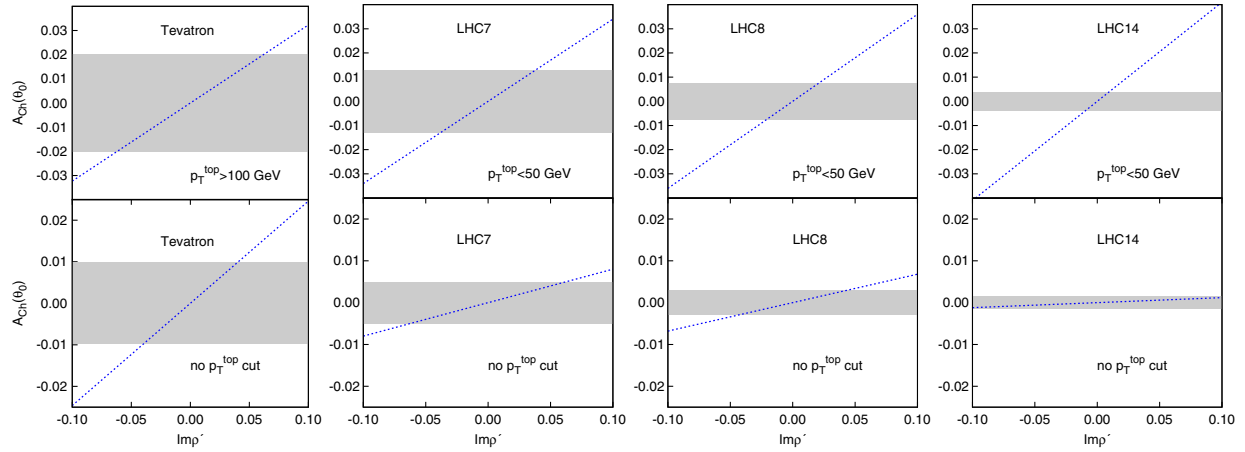


FIG. 6 (color online). The charge asymmetry $A_{\text{ch}}(\theta_0)$ as a function of charged lepton in top-pair production at the Tevatron (bottom left), LHC7 (bottom right), LHC8 (top left) and LHC14 (top right) for anomalous ttg coupling $\text{Im}\rho'$ for $\theta_0 = \pi/8$. The grey band shows the 3 sigma error interval in the SM with the appropriate p_T cut.

that the deviation in the cross section is relatively large in the range $[\pi/8, 3\pi/8]$. To optimize the charge asymmetry of lepton, we choose the cutoff angle θ_0 to be $\pi/8$ and evaluate the asymmetry as a function of $\text{Im}\rho'$. In Fig. 6, we plot the charge asymmetry of the lepton as defined in Eq. (14) as a function of $\text{Im}\rho'$ for chosen value $\pi/8$ of θ_0 for Tevatron, LHC7, LHC8 and LHC14.

We also study the effect of top- p_T cuts on the lepton charge asymmetry $A_{\text{SM}}(\theta_0)$. From the top panel of Fig. 5, we see that at the LHC, keeping low p_T top/antitop would help in enhancing $A_{\text{SM}}(\theta_0)$ while at the Tevatron, the reverse is true. So, we put a cut on top/antitop $p_T < 50$ GeV

at the LHC and $p_T > 100$ GeV at the Tevatron. We show the effects of these p_T cuts on charge asymmetry in top panel of Fig. 6. We find that though the statistical uncertainties increase due to the reduction in number of events, the asymmetry is increased enough times to compensate the reduction in events and thus results in the enhancement of the limits obtained by $A_{\text{SM}}(\theta_0)$ on $\text{Im}\rho'$.

D. Azimuthal asymmetry

As can be seen from Fig. 4, the curves are well separated at the peaks for the chosen values of the anomalous ttg

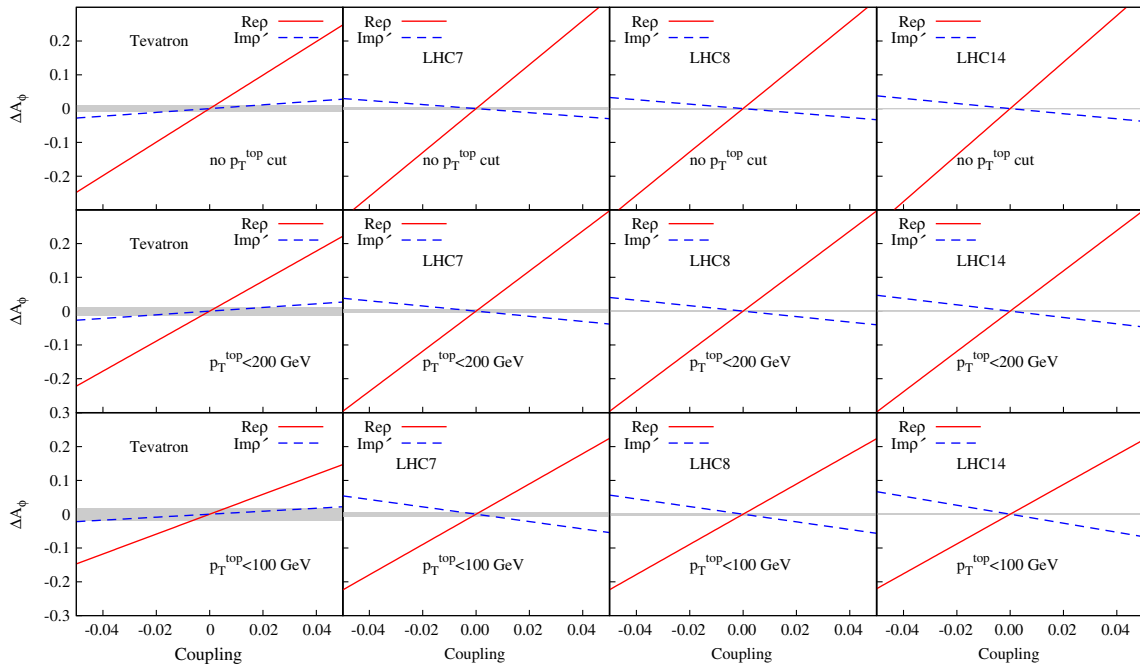


FIG. 7 (color online). The azimuthal asymmetry of the charged lepton in $t\bar{t}$ production at the Tevatron (1st column), LHC7 (2nd column), LHC8 (3rd column) and LHC14 (4th column) for different anomalous ttg couplings. The grey band shows the 3 sigma error interval in the SM with the appropriate p_T cut.

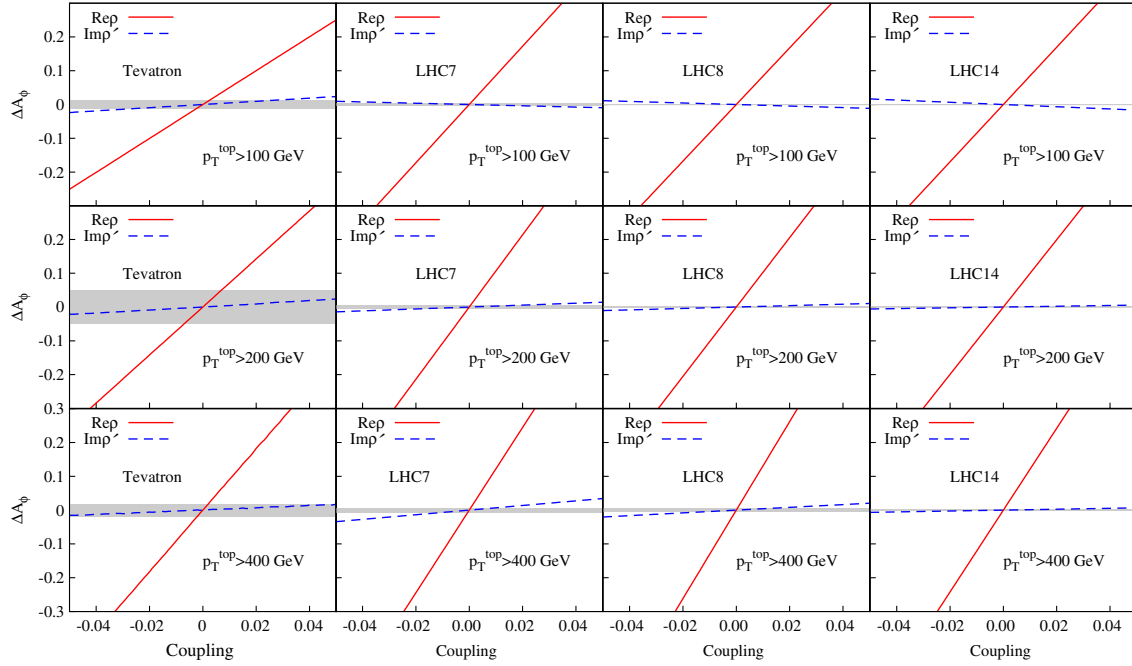


FIG. 8 (color online). The azimuthal asymmetry of the charged lepton in $t\bar{t}$ production at the Tevatron (bottom left), LHC7 (bottom right), LHC8 (top left) and LHC14 (top right) for different anomalous ttg couplings. The grey band shows the 3 sigma error interval in the SM with the appropriate p_T cut.

couplings and are also well separated from the curve for the SM. We define an azimuthal asymmetry for the lepton to quantify these differences in the distributions by

$$A_\phi = \frac{\sigma(\cos \phi_\ell > 0) - \sigma(\cos \phi_\ell < 0)}{\sigma(\cos \phi_\ell > 0) + \sigma(\cos \phi_\ell < 0)}, \quad (15)$$

where the denominator is the total cross section. This azimuthal asymmetry is in fact the “left-right asymmetry” of the charged lepton at the LHC defined with respect to the beam direction, with the right hemisphere defined as that in which the top momentum lies, and the left one being the opposite one. Plots of A_ϕ as a function of the couplings are shown in Figs. 7 and 8 for Tevatron, LHC7, LHC8 and LHC14.

From Fig. 4, we see that the azimuthal distribution of the decay charged lepton is more sensitive to $\text{Re}\rho$ than to $\text{Im}\rho'$. Hence, we expect that the azimuthal asymmetry we construct in Eq. (15) would be a sensitive probe of $\text{Re}\rho$. This fact can indeed be seen from Figs. 7 and 8, where the straight line for $\text{Re}\rho$ is steeper than for $\text{Im}\rho'$, implying a more significant contribution from the former. The reason we get straight lines for individual contributions to the asymmetry is that we are working in a linear approximation for the anomalous couplings.

As mentioned earlier in the context of distributions, the dependence on the two couplings can be separated by choosing the sum and difference of the azimuthal asymmetries for t and \bar{t} . The difference being CP odd, would be dependent only on $\text{Im}\rho'$.

We also study the behavior of A_ϕ in the presence of cuts on the top transverse momentum. In the top panel of the

Fig. 7, we show the behavior of A_ϕ as functions of $\text{Re}\rho$ and $\text{Im}\rho'$ with no cut on the top transverse momentum. In the middle and lower panel, we show A_ϕ when we consider tops with $p_T < 100$ and 200 GeV, respectively. Similarly in Fig. 8 we consider high- p_T tops to evaluate the asymmetry. In the top, the middle and the lower panel of Fig. 8, we show A_ϕ as functions of $\text{Re}\rho$ and $\text{Im}\rho'$ for top quarks with $p_T > 100$, 200 and 400 GeV, respectively.

We find that for high- p_T tops, the azimuthal distribution is relatively more peaked than for low- p_T ones. The reason for this is the $(1 - \beta_t \cos \theta_{t\ell})^3$ factor in the denominator of Eqs. (11) and (12). Thus, when β_t is large, the distribution tends to peak near 0 and 2π . As a result asymmetry A_ϕ is larger for high- p_T tops. This effect can be seen from Figs. 7 and 8 where it can be easily seen that as the p_T of the top is increased, the azimuthal asymmetry is larger. Hence we conclude that asymmetry constructed from high- p_T tops would be more useful in constraining the anomalous top-gluon couplings. From the Fig. 8 we see that the coupling $\text{Re}\rho$ is more sensitive at the Tevatron and LHC14. Though the value of the asymmetry also increases for lower- p_T tops, the statistics is very low in that region and thus we do not gain in sensitivity.

IV. SENSITIVITY ANALYSIS FOR ANOMALOUS ttg COUPLINGS

We now study the statistical significance of the observables discussed in the previous sections to the anomalous ttg couplings at the Tevatron, LHC7, LHC8 and LHC14.

For Tevatron, LHC7, LHC8 and LHC14, we assume integrated luminosities of 8 fb^{-1} , 5 fb^{-1} , 10 fb^{-1} , and 10 fb^{-1} , respectively. To obtain the 3σ limit on the anomalous ttg couplings from a measurement of an observable, we find those values of the couplings for which the observable deviates by 3σ from its SM value. The statistical uncertainty σ_i in the measurement of any generic asymmetry \mathcal{A}_i is given by

$$\sigma_i = \sqrt{\frac{1 - (\mathcal{A}_i^{\text{SM}})^2}{\mathcal{N}}}, \quad (16)$$

where $\mathcal{A}_i^{\text{SM}}$ is the asymmetry predicted in the SM and \mathcal{N} is the total number of events predicted in the SM. We apply this to the various asymmetries we have discussed. In case of the top polarization asymmetry, the limits are obtained on the assumption that the polarization can be measured with 100% accuracy. When lepton angular variables are used, their intrinsic efficiency to measure top polarization is already built in our formalism. We do not take into account cuts which may be needed for reducing background events. This may result in some loss of efficiency, which we have not attempted to estimate.

The 3σ limits on $\text{Re}\rho$ and $\text{Im}\rho'$ are given in Table I where we assume only one anomalous coupling to be nonzero at a time. In case of the lepton distributions, we take into account only one leptonic channel. Including other leptonic decays of the top would improve the limits further.

In Table II, we give the 3σ limits on $\text{Re}\rho$ and $\text{Im}\rho'$ applying a cut $p_T < 100 \text{ GeV}$ on the top transverse momentum. From the table, we find that though the asymmetry increases for $\text{Im}\rho'$ with the cut, the limits on it

do not change much because of the opposite effect of reduction in statistics. On the other hand, the limits on $\text{Re}\rho$ actually worsen because the top- p_T cut reduces the asymmetry for $\text{Re}\rho$.

In Table III, we give the 3σ limits on $\text{Re}\rho$ and $\text{Im}\rho'$ applying a cut $p_T > 100 \text{ GeV}$. From the table, we find that with this cut, the limits are more stringent for $\text{Re}\rho$ since the asymmetry A_ϕ for it is steeper as compared to the value without cuts. On the other hand, the limits on $\text{Im}\rho'$ actually worsen because the top- p_T cut reduces the asymmetry.

We also obtain simultaneous limits (taking both $\text{Re}\rho$ and $\text{Im}\rho'$ nonzero simultaneously) on these anomalous couplings that may be obtained by combining the measurements at Tevatron with LHC7, LHC8 and LHC14.

For this, we perform a χ^2 analysis to fit all the observables to within $f\sigma$ of statistical errors in the measurement of the observable. We define the following χ^2 function

$$\chi^2 = \sum_{i=1}^n \left(\frac{P_i - O_i}{\sigma_i} \right)^2, \quad (17)$$

where the sum runs over the n observables measured and f is the degree of the confidence interval. P_i 's are the values of the observables obtained by taking both anomalous couplings nonzero (and is a function of the couplings $\text{Re}\rho$ and $\text{Im}\rho'$) and O_i 's are the values of the observables obtained in the SM. σ_i 's are the statistical fluctuations in the measurement of the observables, given in Eq. (16).

In Fig. 9, we show the 1σ , 2σ and 3σ regions in $\text{Re}\rho$ - $\text{Im}\rho'$ plane allowed by combined measurement of asymmetry A_ϕ at different experiments, taken two at a time. For this, in the χ^2 function of Eq. (17), we have

TABLE I. Individual limits on anomalous couplings $\text{Re}\rho$ and $\text{Im}\rho'$ which may be obtained by the measurement of the observables at Tevatron, LHC7, LHC8 and LHC14 with integrated luminosities of 8, 5, 10, and 10 fb^{-1} respectively.

	P_t	A_ϕ		$A_{\text{ch}}(\theta_0 = \pi/8)$
		$\text{Re}\rho$	$\text{Im}\rho'$	$\text{Im}\rho'$
Tevatron	$[-9.75, 9.75] \times 10^{-3}$	$[-2.22, 2.22] \times 10^{-2}$	$[-1.96, 1.96] \times 10^{-2}$	$[-3.98, 3.98] \times 10^{-2}$
LHC7	$[-2.10, 2.10] \times 10^{-3}$	$[-1.43, 1.43] \times 10^{-3}$	$[-6.52, 6.52] \times 10^{-3}$	$[-6.25, 6.25] \times 10^{-2}$
LHC8	$[-1.06, 1.06] \times 10^{-3}$	$[-3.58, 3.58] \times 10^{-4}$	$[-3.50, 3.50] \times 10^{-3}$	$[-4.41, 4.41] \times 10^{-2}$
LHC14	$[-5.59, 5.59] \times 10^{-4}$	$[-1.60, 1.60] \times 10^{-4}$	$[-1.46, 1.46] \times 10^{-3}$	$[-1.25, 1.25] \times 10^{-1}$

TABLE II. Individual limits on anomalous couplings $\text{Re}\rho$ and $\text{Im}\rho'$, with a cut $p_T < 100 \text{ GeV}$ on the top transverse momentum (for A_{ch} , we take $p_T < 50 \text{ GeV}$), which may be obtained by the measurement of the observables at Tevatron, LHC7, LHC8 and LHC14 with integrated luminosities of 8, 5, 10, and 10 fb^{-1} , respectively.

	P_t	A_ϕ		$A_{\text{ch}}(\theta_0 = \pi/8)$
		$\text{Re}\rho$	$\text{Im}\rho'$	$\text{Im}\rho'$
Tevatron	$[-1.50, 1.50] \times 10^{-2}$	$[-6.12, 6.12] \times 10^{-3}$	$[-4.09, 4.09] \times 10^{-2}$	—
LHC7	$[-1.22, 1.22] \times 10^{-3}$	$[-1.45, 1.45] \times 10^{-3}$	$[-5.98, 5.98] \times 10^{-3}$	$[-3.82, 3.82] \times 10^{-2}$
LHC8	$[-6.22, 6.22] \times 10^{-4}$	$[-8.97, 8.97] \times 10^{-4}$	$[-3.55, 3.55] \times 10^{-3}$	$[-2.14, 2.14] \times 10^{-2}$
LHC14	$[-2.85, 2.85] \times 10^{-4}$	$[-4.30, 4.30] \times 10^{-4}$	$[-1.43, 1.43] \times 10^{-3}$	$[-9.76, 9.76] \times 10^{-3}$

TABLE III. Individual limits on anomalous couplings $\text{Re}\rho$ and $\text{Im}\rho'$, with a cut $p_T > 100$ GeV on the top transverse momentum, which may be obtained by the measurement of the observables at Tevatron, LHC7, LHC8 and LHC14 with integrated luminosities of 8, 5, 10, and 10 fb^{-1} , respectively.

	P_t	A_ϕ		$A_{\text{ch}}(\theta_0 = \pi/8)$
	$\text{Im}\rho'$	$\text{Re}\rho$	$\text{Im}\rho'$	$\text{Im}\rho'$
Tevatron	$[-6.79, 6.79] \times 10^{-3}$	$[-1.22, 1.22] \times 10^{-3}$	$[-1.87, 1.87] \times 10^{-2}$	$[-6.19, 6.19] \times 10^{-2}$
LHC7	$[-6.90, 6.90] \times 10^{-3}$	$[-4.64, 4.64] \times 10^{-4}$	$[-4.44, 4.44] \times 10^{-2}$	–
LHC8	$[-1.94, 1.94] \times 10^{-3}$	$[-2.86, 2.86] \times 10^{-4}$	$[-1.05, 1.05] \times 10^{-2}$	–
LHC14	$[-1.08, 1.08] \times 10^{-3}$	$[-1.30, 1.30] \times 10^{-4}$	$[-3.33, 3.33] \times 10^{-3}$	–

combined the measurement at Tevatron with the measurements at LHC7, LHC8 and LHC14. From among the three combinations shown in Fig. 9, we find that the strongest simultaneous limits come from the combined measurements at Tevatron and LHC14, viz., ± 0.006 on $\text{Re}\rho$ and ± 0.04 on $\text{Im}\rho'$, at the 3σ level.

We now describe some other relevant work on the determination of the chromomagnetic and chromoelectric form factors of the top at hadron colliders. Some earlier work [26–28] made projections for possible limits on the couplings which would be obtained at the Tevatron and the LHC. In Ref. [28], the authors study polar-angle, transverse momentum and energy distributions of charged leptons coming from top decay at the Tevatron and LHC. Our results on polar-angle distributions of charged leptons are in agreement with theirs for nonzero $\text{Re}\rho$. They find 10%–15% deviations from the SM in the angular distributions for values of ρ around 0.01 and of ρ' around 0.05. They also study lepton energy distributions, which bring in dependence on anomalous tbW couplings. Refs. [26,27] proposed utilizing cross section measurements at the LHC and the Tevatron to put limits on the anomalous couplings. With the available data from Tevatron, Choudhury *et al.* [29], using a slightly different notation, put limits on the new physics scale Λ . They conclude that the cross section measurements at Tevatron would put a lower bound on Λ of about 7.4 and 9 TeV for $\rho = \pm 1$, respectively, which in

our notation would translate to $\rho \sim [-1.94, 2.36] \times 10^{-2}$, while at LHC7 the lower bound on Λ is 10 TeV, which is equivalent to $\rho < 1.75 \times 10^{-2}$. Hioki and Ohkuma [30] in their work, which they consider an update of [27], find that the Tevatron cross section results give bounds $-0.01 < \rho < 0.01$ and $0.38 < \rho < 0.41$ and $|\rho'| < 0.12$, of which, only the region around $\rho = 0$ and $\rho' = 0$ survive on using early LHC data. They also studied the effect on top p_T , polar-angle distributions and invariant mass distributions from various combinations of ρ and ρ' in the range of 0.1–0.4 and found them to give significant deviations from SM predictions. Hesari and Najafabadi [31] studied the fraction of the gg fusion contribution in $t\bar{t}$ production cross section at the Tevatron and at the LHC and concluded that this fraction is more sensitive at the Tevatron than at the LHC. From Tevatron results with integrated luminosity of 1 fb^{-1} , they quote limits of $1.1 < \rho < 0.6$, $0.8 < \rho' < 0.8$. For the full luminosity accumulated at the Tevatron, they project limits of $0.03 < \rho < 1.5$ and $0.37 < \rho' < 0.37$, while at the LHC7, the limits they expect are $0.04 < \rho < 0.98$ and $0.15 < \rho' < 0.15$. They also studied the charge asymmetry of the top at the LHC and found very loose bounds on ρ from it, and no sensitivity to ρ' .

Other authors have considered possible limits on couplings from more detailed observations. In Refs. [32], the authors considered probing the CP -violating chromoelectric dipole moment utilizing T-odd correlations constructed

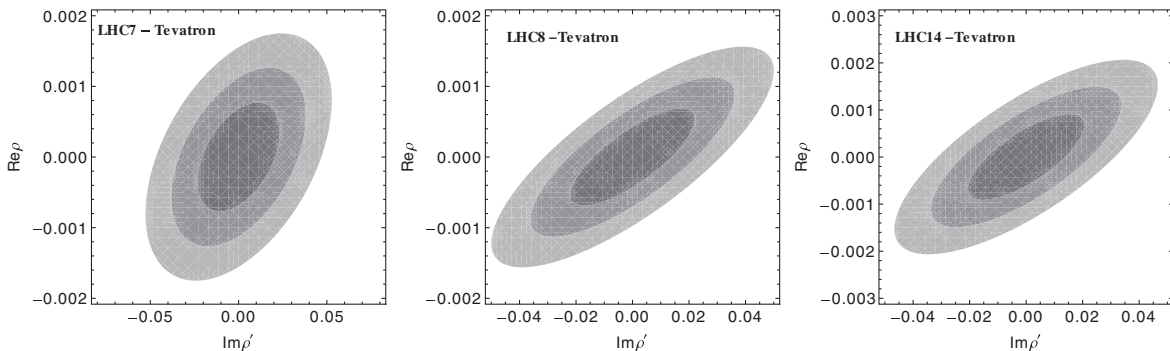


FIG. 9. The 1σ (central region), 2σ (middle region) and 3σ (outer region) CL regions in the $\text{Re}\rho$ - $\text{Im}\rho'$ plane allowed by the combined measurement of two observables at a time. The left, center and right plots correspond to measurements at the combinations Tevatron-LHC7, Tevatron-LHC8 and Tevatron-LHC14, respectively. The χ^2 values for 1σ , 2σ and 3σ CL intervals are 2.30, 6.18 and 11.83, respectively, for two parameters in the fit.

from jet and lepton momenta and found the expected limit to be $|\rho'| < 5 \times 10^{-3}$. Reference [33] studies the chromoelectric coupling utilizing various momentum correlations in $t\bar{t}$ and $t\bar{t}$ plus one-jet processes and derives the limit of $|\rho'| \geq 0.35$. In Ref. [34] Rizzo studied anomalous ttg couplings in single-top production at the Tevatron and at the LHC and concluded that the limits from this channel are about one order of magnitude smaller than those from the pair production processes. Effect of ρ and ρ' on spin correlations in $t\bar{t}$ has been studied in Ref. [35], and bounds are found to be $-0.7 < \rho < 0.6$ and $-0.5 < \rho' < 0.5$.

In all above papers, authors have considered anomalous ttg couplings to be real. We consider both chromomagnetic and chromoelectric form factors to be complex. We found, however, that our observables get contributions only from the real part of ρ and the imaginary part of ρ' . The projections for the best limits on $\text{Re}\rho$ from our observables are sometimes an order of magnitude better than those obtained from cross sections. In our analysis, we found top polarization and charge asymmetry of the charged lepton (both of which are CP odd) to be dependent on the imaginary part of the chromoelectric form factor. In Ref. [36], the author has considered chromomagnetic and chromoelectric form factors to be complex and construct various CP -violating observables to obtain constraints on real and imaginary parts of ρ' . At the Tevatron with 30 fb^{-1} , the author obtained limits of $2.4 \times 10^{-18} \text{ cm } g_s$ and $1.1 \times 10^{-18} \text{ cm } g_s$ on $\text{Re}\rho'$ and $\text{Im}\rho'$, respectively, which in our units translate to 2.13×10^{-2} and 9.77×10^{-3} . At LHC14 with 150 fb^{-1} , the limits obtained are $5.2 \times 10^{-20} \text{ cm } g_s$ and $2.5 \times 10^{-20} \text{ cm } g_s$ on $\text{Re}\rho'$ and $\text{Im}\rho'$, respectively. In our units, limits are 4.62×10^{-3} and 1.91×10^{-3} on $\text{Re}\rho'$ and $\text{Im}\rho'$, respectively. Considering that the luminosities we use for our limits are much lower, our limits are comparable to theirs.

More recently, Ref. [43] has obtained upper bounds on chromomagnetic dipole moment ($\text{Re}\rho$) as 0.085 using the available data for the cross sections for $t\bar{t}$ production at Tevatron and LHC for 7 TeV. They have predicted that the sensitivity to probe this coupling will be improved by a factor upto 4 by the boosted top measurements at 14 TeV LHC.

V. CONCLUSIONS

We have investigated the sensitivity of the Tevatron, LHC7, LHC8 and LHC14 to the anomalous ttg couplings in top-pair production followed by semileptonic decay of the top. We derived analytical expressions for the spin density matrix for top-quark production including the contributions of both real and imaginary parts of anomalous ttg couplings. We evaluate these at leading order in the strong coupling, and neglect electroweak contributions. We work in the linear approximation of anomalous couplings. We find that only $\text{Re}\rho$ and $\text{Im}\rho'$ give significant contributions to the spin density matrix at linear order. It

may be noted that $\text{Im}\rho$ and $\text{Re}\rho'$ do not appear in the observables we consider. This may be understood from the fact that the observables are even under naive time reversal T , viz., under change of sign of all the momenta and spins, without an interchange of initial and final states. In such a case, from the CPT theorem, the observables which are CP even can only arise from dispersive parts of form factors (in this case $\text{Re}\rho$) and the CP -odd observable can arise only from absorptive parts (in this case $\text{Im}\rho'$).

Longitudinal top polarization can be utilized to separate the contribution of $\text{Im}\rho'$ completely independent of all other anomalous couplings whereas the total cross section can be used to separate the contribution of $\text{Re}\rho$.

Since top polarization can be measured only through the differential distribution of its decay products, we also study the angular distributions of the charged lepton coming from the decay of the top. Charged-lepton momenta are measurable very accurately at the LHC and charged leptons have the best spin analyzing power. Also, charged-lepton angular distributions have been shown to be independent of any NP in top decay. We find that the polar-angle distribution is not very sensitive to the anomalous couplings. On the other hand, the normalized azimuthal distribution is found to be sensitive to the anomalous couplings. The azimuthal distribution peaks close to $\phi = 0$ and $\phi = 2\pi$, and the values at the peaks are quite sensitive to the magnitude and the sign of the anomalous couplings. In order to quantify this difference and to be statistically more sensitive, we construct an integrated azimuthal asymmetry from the azimuthal distribution of charged lepton.

We study the effects of top transverse momentum cuts on top polarization and azimuthal distributions. We find that the top p_T cut may enhance or reduce the top polarization depending on whether we take a sample of low- p_T or high- p_T tops. In our analysis, we observed that for the Tevatron an ensemble of high- p_T tops have higher degree of longitudinal top polarization as the function of imaginary part of anomalous chromoelectric coupling ρ' . Conversely, an ensemble of low- p_T tops reduce the top polarization at Tevatron for nonzero $\text{Im}\rho'$. On the other hand, in the case of the LHC, the observation is reversed. For high- p_T tops, top polarization is small and vice versa.

We consider two angular asymmetries, leptonic charge asymmetry $A_{\text{ch}}(\theta_0)$ and leptonic left-right asymmetry A_ϕ , which serve as measures of the anomalous couplings. We find that the $A_{\text{ch}}(\theta_0)$ is proportional to $\text{Im}\rho'$. The difference in the ℓ^+ and ℓ^- cross sections is relatively large in the range θ_0 : $[\pi/8, 3\pi/8]$. We choose the cutoff θ_0 to be $\pi/8$ to maximize the $A_{\text{ch}}(\theta_0)$. We furthermore study the effects of top p_T cuts on the charge asymmetry and conclude that $A_{\text{ch}}(\theta_0)$ is enhanced in the low top- p_T region at the LHC while the reverse is true for Tevatron.

The effect of top p_T cuts on the angular distribution of charged leptons can be easily understood through Eq. (10). For high- p_T tops, the angular distributions peak at extreme

values leading to larger azimuthal asymmetries A_ϕ . We also study the effect of these cuts on the limits obtained by the measurement of top polarization and azimuthal asymmetry. We infer that the high- p_T tops give large azimuthal asymmetries and can thus give more stringent limits on the chromomagnetic top-gluon coupling as compared to low- p_T tops.

We have restricted ourselves to an analysis of the statistical sensitivities and not done a detailed analysis of the effects of cuts needed for discrimination against background and of detector efficiencies. Such an analysis would be required for a more precise determination of the sensitivities of our observables. In conclusion, we have shown that top polarization, and subsequent decay-lepton distributions can be used to obtain fairly stringent limits on chromomagnetic and chromoelectric top couplings from the existing Tevatron data as well as data soon to be available after the 8 TeV run of the LHC. The limits could be improved by the future runs of the LHC.

ACKNOWLEDGMENTS

S. D. R. thanks the Theoretical Physics Department of Tata Institute of Fundamental Research for hospitality during the beginning of this work, and the Korea Institute for Advanced Study, Seoul, for hospitality during the conclusion of the work. He also acknowledges financial support from the Department of Science and Technology, India, in the form of the J. C. Bose National Fellowship, Grant No. SR/S2/JCB-42/2009. We thank Namit Mahajan for pointing out an error in an earlier version of the manuscript.

APPENDIX: SPIN DENSITY MATRIX FOR TOP/ANTITOP IN TOP-PAIR PRODUCTION WITH ANOMALOUS ttg COUPLINGS

In this appendix, we present the spin density matrix elements σ^{ij} for the top quark in the top-pair production process. We include contributions of all anomalous couplings to linear order.

Some general considerations can be used to anticipate the structure of the density matrix. Writing the density matrix as a sum of various contributions, σ_{SM} from the SM, and $\sigma_{\text{Re}\rho, \text{Re}\rho', \text{Im}\rho, \text{Im}\rho'}$, the respective contributions from $\text{Re}\rho$, $\text{Re}\rho'$, $\text{Im}\rho$ and $\text{Im}\rho'$,

$$\sigma^{ij} = \sigma_{\text{SM}}^{ij} + \sigma_{\text{Re}\rho}^{ij} + \sigma_{\text{Re}\rho'}^{ij} + \sigma_{\text{Im}\rho}^{ij} + \sigma_{\text{Im}\rho'}^{ij}. \quad (\text{A1})$$

Then, Hermiticity of the density matrix gives

$$\sigma^{\pm\pm} = \sigma^{\pm\pm*}, \quad (\text{A2})$$

implying that the diagonal matrix elements are real, and

$$\text{Re } \sigma^{\pm\mp} = \text{Re } \sigma^{\mp\pm} \quad \text{Im } \sigma^{\pm\mp} = -\text{Im } \sigma^{\mp\pm}. \quad (\text{A3})$$

Thus, the only imaginary contributions come in the off-diagonal elements, changing sign under helicity flip.

Let us now see what transformation under naive time reversal T tells us. Under T , σ^{ij} is transformed to σ^{ij*} . We note that ρ' terms are odd under CP , and therefore under T . Hence terms with $\text{Re}\rho'$ would change sign under T . However, since T does not interchange initial and final states, the contribution from $\text{Im}\rho'$ does not change sign, as it arises from the absorptive part of some amplitude in the underlying theory. By the same argument, the $\text{Im}\rho$ term changes sign under T , even though the corresponding interaction is T invariant. We thus have the relations

$$\begin{aligned} \sigma_{\text{Re}\rho'}^{\pm\pm} &= \sigma_{\text{Im}\rho}^{\pm\pm} = 0, & \text{Re } \sigma_{\text{Re}\rho'}^{\pm\mp} &= \text{Re } \sigma_{\text{Im}\rho}^{\pm\mp} = 0, \\ \text{Im } \sigma_{\text{SM}}^{\pm\mp} &= \text{Im } \sigma_{\text{Re}\rho}^{\pm\mp} = \text{Im } \sigma_{\text{Im}\rho'}^{\pm\mp} = 0. \end{aligned} \quad (\text{A4})$$

Thus, the diagonal density matrix elements can depend only on the couplings $\text{Re}\rho$ and $\text{Im}\rho'$.

The following relations arise from the parity transformation P , which flips the signs of the helicities, using the fact that the ρ' couplings are odd under P , and that there is an extra phase factor of -1 in the transformation of the off-diagonal elements:

$$\begin{aligned} \sigma_{\text{SM}}^{\pm\pm} &= \sigma_{\text{SM}}^{\mp\mp}, & \sigma_{\text{Re}\rho}^{\pm\pm} &= \sigma_{\text{Re}\rho}^{\mp\mp}, \\ \sigma_{\text{Im}\rho'}^{\pm\pm} &= -\sigma_{\text{Im}\rho'}^{\mp\mp}, & \text{Re } \sigma_{\text{SM}}^{\pm\mp} &= -\text{Re } \sigma_{\text{SM}}^{\mp\pm}, \\ \text{Re } \sigma_{\text{Re}\rho}^{\pm\mp} &= -\text{Re } \sigma_{\text{Re}\rho'}^{\mp\pm}, & \text{Re } \sigma_{\text{Im}\rho'}^{\pm\mp} &= \text{Re } \sigma_{\text{Im}\rho'}^{\mp\pm}, \\ \text{Im } \sigma_{\text{Im}\rho}^{\pm\mp} &= -\text{Im } \sigma_{\text{Im}\rho'}^{\mp\pm}, & \text{Im } \sigma_{\text{Re}\rho'}^{\pm\mp} &= \text{Im } \sigma_{\text{Re}\rho}^{\mp\pm}. \end{aligned} \quad (\text{A5})$$

Now the above equations, together with the Hermiticity relations in Eq. (A3) tell us that

$$\text{Re } \sigma_{\text{SM}}^{\pm\mp} = 0, \quad \text{Re } \sigma_{\text{Re}\rho}^{\pm\mp} = 0, \quad \text{Im } \sigma_{\text{Re}\rho'}^{\pm\mp} = 0. \quad (\text{A6})$$

We conclude from the above that the diagonal matrix elements, which are all real, can only get contributions from the SM, and from $\text{Re}\rho$ and $\text{Im}\rho'$. The off-diagonal elements have no contribution from the SM (since the SM amplitudes are real at tree level), and get a real contribution from $\text{Im}\rho'$ and an imaginary contribution from $\text{Im}\rho$. Also, the $\text{Im}\rho'$ contribution in the diagonal elements and the $\text{Im}\rho$ contribution in the off-diagonal elements change sign under helicity flip.

The density matrix $\bar{\sigma}$ for the spin of the top antiquark is obtained by changing the sign of the $\text{Im}\rho$ and $\text{Im}\rho'$ terms only in the off-diagonal element of the spin density matrix for the top quark. This can be seen from the fact that under the operation of CPT , where T is naive time reversal (reversing the sign of all spins and momenta, without interchange of initial and final states), the top spin density matrix elements would be transformed to the complex conjugates of the corresponding antitop spin density matrix elements, with the helicity indices changing sign. However, this applies only to the real parts of couplings. Contributions containing imaginary parts of anomalous

couplings, which arise from absorptive parts of amplitudes in an underlying theory, would change sign under this operation. Thus, because of *CPT* invariance,

$$\bar{\sigma}_{\text{SM}}^{\pm\pm} = \sigma_{\text{SM}}^{\mp\mp} = \sigma_{\text{SM}}^{\pm\pm} \quad (\text{A7})$$

$$\bar{\sigma}_{\text{Re}\rho}^{\pm\pm} = \sigma_{\text{Re}\rho}^{\mp\mp} = \sigma_{\text{Re}\rho}^{\pm\pm} \quad (\text{A8})$$

$$\bar{\sigma}_{\text{Im}\rho'}^{\pm\pm} = -\sigma_{\text{Im}\rho'}^{\mp\mp} = \sigma_{\text{Im}\rho'}^{\pm\pm} \quad (\text{A9})$$

$$\text{Im } \bar{\sigma}_{\text{Im}\rho}^{\pm\mp} = \text{Im } \sigma_{\text{Im}\rho}^{\mp\pm} = -\text{Im } \sigma_{\text{Im}\rho}^{\pm\mp} \quad (\text{A10})$$

$$\text{Re } \bar{\sigma}_{\text{Im}\rho'}^{\pm\mp} = -\text{Re } \sigma_{\text{Im}\rho'}^{\mp\pm} = -\text{Re } \sigma_{\text{Im}\rho'}^{\pm\mp} \quad (\text{A11})$$

We denote the spin density matrix for the top quark in the $q\bar{q}$ -initiated process as $\sigma_{q\bar{q}}^{\lambda\lambda'}$ and that for the gluon-gluon fusion process as $\sigma_{gg}^{\lambda\lambda'}$. The labels (in subscript) s, t, u in $\sigma_{gg}^{\lambda\lambda'}$ denote the s, t and u channel contributions, respectively, whereas st, su and tu denote the interference between s and t channels, s and u channels and t and u channels, respectively. The λ and λ' are top helicities and may take values \pm . The total contribution of four-point $ggtt$ couplings is included in the terms corresponding to the interference of the s -channel exchange amplitude with the t - and u -channel exchange amplitudes with a coefficient labelled by g^* and later set to 1. The spin-density matrix elements $\sigma^{\lambda\lambda'}$ for top quark in $t\bar{t}$ -pair production in the parton cm frame (at parton level) are written as

$$\begin{aligned} \sigma^{++} &= \sigma_{q\bar{q}}^{++} + \sigma_{gg,s}^{++} + \sigma_{gg,t}^{++} + \sigma_{gg,u}^{++} \\ &\quad + \sigma_{gg,st}^{++} + \sigma_{gg,su}^{++} + \sigma_{gg,tu}^{++} \end{aligned} \quad (\text{A12})$$

$$\begin{aligned} \sigma^{+-} &= \sigma_{q\bar{q}}^{+-} + \sigma_{gg,s}^{+-} + \sigma_{gg,t}^{+-} + \sigma_{gg,u}^{+-} \\ &\quad + \sigma_{gg,st}^{+-} + \sigma_{gg,su}^{+-} + \sigma_{gg,tu}^{+-} \end{aligned} \quad (\text{A13})$$

$$\begin{aligned} \sigma^{-+} &= \sigma_{q\bar{q}}^{-+} + \sigma_{gg,s}^{-+} + \sigma_{gg,t}^{-+} + \sigma_{gg,u}^{-+} \\ &\quad + \sigma_{gg,st}^{-+} + \sigma_{gg,su}^{-+} + \sigma_{gg,tu}^{-+} \end{aligned} \quad (\text{A14})$$

$$\begin{aligned} \sigma^{--} &= \sigma_{q\bar{q}}^{--} + \sigma_{gg,s}^{--} + \sigma_{gg,t}^{--} + \sigma_{gg,u}^{--} \\ &\quad + \sigma_{gg,st}^{--} + \sigma_{gg,su}^{--} + \sigma_{gg,tu}^{--} \end{aligned} \quad (\text{A15})$$

where

$$\begin{aligned} \sigma_{q\bar{q}}^{\pm\pm} &= 2C_{q\bar{q}}\hat{s}^2[16\text{Re}\rho \pm 8\text{Im}\rho' \beta_t \sin^2\theta_t \\ &\quad + 1 + \beta_t^2 \cos^2\theta_t + 4r_t] \end{aligned} \quad (\text{A16})$$

$$\sigma_{q\bar{q}}^{\pm\mp} = \frac{4C_{q\bar{q}}}{m_t} \hat{s}^2 \sqrt{\hat{s}} \sin 2\theta_t \beta_t [\mp i \text{Im}\rho \beta_t + \text{Im}\rho'] \quad (\text{A17})$$

$$\sigma_{gg,s}^{\pm\pm} = 2C_s \hat{s}^2 [8\text{Re}\rho \pm 8\text{Im}\rho' \beta_t \cos^2\theta_t + (1 - \beta_t^2 \cos^2\theta_t)] \quad (\text{A18})$$

$$\sigma_{gg,s}^{\pm\mp} = -\frac{4C_s}{m_t} \hat{s}^2 \sqrt{\hat{s}} \sin 2\theta_t \beta_t [\pm i \text{Im}\rho \beta_t + \text{Im}\rho'] \quad (\text{A19})$$

$$\begin{aligned} \sigma_{gg,t}^{\pm\pm} &= C_t \hat{s}^2 [16\text{Re}\rho(1 - \beta_t \cos\theta_t) \pm 4\text{Im}\rho' \{\beta_t(1 - 8r_t) \\ &\quad - \cos\theta_t(1 + 12r_t) + \beta_t \cos^2\theta_t(1 + 16r_t) \\ &\quad - 3\beta_t^2 \cos^3\theta_t + 2\beta_t^3 \cos^4\theta_t\} + 1 + 4r_t - 16r_t^2 \\ &\quad - \beta_t^3 \cos\theta_t - 8\beta_t^2 r_t \cos^2\theta_t + \beta_t^3 \cos^3\theta_t - \beta_t^4 \cos^4\theta_t] \end{aligned} \quad (\text{A20})$$

$$\begin{aligned} \sigma_{gg,t}^{\pm\mp} &= \frac{2C_t}{m_t} \hat{s}^2 \sqrt{\hat{s}} \sin\theta_t [(\text{Im}\rho' \pm i\beta_t \text{Im}\rho) \\ &\quad \times \{1 + 8r_t - 2\beta_t \cos\theta_t - 8\beta_t \cos\theta_t r_t + 3\beta_t^2 \cos^2\theta_t \\ &\quad - 2\beta_t^3 \cos^3\theta_t\} + 4r_t \text{Im}\rho' \{1 - \beta_t \cos\theta_t\}] \end{aligned} \quad (\text{A21})$$

$$\begin{aligned} \sigma_{gg,u}^{\pm\pm} &= C_u \hat{s}^2 [16\text{Re}\rho(1 + \beta_t \cos\theta_t) \pm 4\text{Im}\rho' \{\beta_t(1 - 8r_t) \\ &\quad + \cos\theta_t(1 + 12r_t) + \beta_t \cos^2\theta_t(1 + 16r_t) \\ &\quad + 3\beta_t^2 \cos^3\theta_t + 2\beta_t^3 \cos^4\theta_t\} + 1 + 4r_t - 16r_t^2 \\ &\quad + \beta_t^3 \cos\theta_t - 8\beta_t^2 r_t \cos^2\theta_t - \beta_t^3 \cos^3\theta_t - \beta_t^4 \cos^4\theta_t] \end{aligned} \quad (\text{A22})$$

$$\begin{aligned} \sigma_{gg,u}^{\pm\mp} &= -\frac{2C_u}{m_t} \hat{s}^2 \sqrt{\hat{s}} \sin\theta_t [(\text{Im}\rho' \pm i\beta_t \text{Im}\rho) \\ &\quad \times \{1 + 8r_t + 2\beta_t \cos\theta_t + 8\beta_t \cos\theta_t r_t + 3\beta_t^2 \cos^2\theta_t \\ &\quad + 2\beta_t^3 \cos^3\theta_t\} + 4r_t \text{Im}\rho' \{1 + \beta_t \cos\theta_t\}] \end{aligned} \quad (\text{A23})$$

$$\begin{aligned} \sigma_{gg,st}^{\pm\pm} &= 2C_{st} \hat{s}^2 [4\text{Re}\rho(3 - (2 + g^*)\beta_t \cos\theta_t) \\ &\quad \mp 4\text{Im}\rho' \cos\theta_t(2 + g^* - 2\beta_t^2 \sin^2\theta_t - 3\beta_t \cos\theta_t) \\ &\quad + 1 - \beta_t^2 \cos^2\theta_t - \beta_t^3 \cos\theta_t \sin^2\theta_t] \end{aligned} \quad (\text{A24})$$

$$\begin{aligned} \sigma_{gg,st}^{\pm\mp} &= \frac{4C_{st}}{m_t} \hat{s}^2 \sqrt{\hat{s}} \sin\theta_t [(\text{Im}\rho' \pm i\beta_t \text{Im}\rho)(1 - 3\beta_t \cos\theta_t \\ &\quad + 2\beta_t^2 \cos^2\theta_t + 4r_t) + 4g^* r_t \text{Im}\rho'] \end{aligned} \quad (\text{A25})$$

$$\begin{aligned} \sigma_{gg,su}^{\pm\pm} &= -2C_{su} \hat{s}^2 [4\text{Re}\rho(3 + (2 + g^*)\beta_t \cos\theta_t) \\ &\quad \pm 4\text{Im}\rho' \cos\theta_t(2 + g^* - 2\beta_t^2 \sin^2\theta_t + 3\beta_t \cos\theta_t) \\ &\quad + 1 - \beta_t^2 \cos^2\theta_t + \beta_t^3 \cos\theta_t \sin^2\theta_t] \end{aligned} \quad (\text{A26})$$

$$\sigma_{gg,su}^{\pm\mp} = -\frac{4C_{su}}{m_t} \hat{s}^2 \sqrt{\hat{s}} \sin \theta_t [(\text{Im} \rho' \pm i \beta_t \text{Im} \rho)(1 + 3\beta_t \cos \theta_t + 2\beta_t^2 \cos^2 \theta_t + 4r_t) + 4g^* r_t \text{Im} \rho'] \quad (\text{A27})$$

$$\sigma_{gg,tu}^{\pm\pm} = 2C_{tu} \hat{s}^2 \sin^2 \theta_t \beta_t [\pm 4 \text{Im} \rho' \{-1 + 2\beta_t^2 \sin^2 \theta_t\} + \beta_t \{1 - \beta_t^2 \sin^2 \theta_t\}] \quad (\text{A28})$$

$$\sigma_{gg,t\bar{u}}^{\pm\mp} = -\frac{4C_{t\bar{u}}}{m_t} \hat{s}^2 \sqrt{\hat{s}} \sin 2\theta_t \beta_t [(\text{Im} \rho' \pm i \beta_t \text{Im} \rho) \times \beta_t^2 \sin^2 \theta_t - 2r_t \text{Im} \rho']. \quad (\text{A29})$$

Here,

$$C_{q\bar{q}} = \frac{g_s^4}{18 \hat{s}^2}; \quad C_s = \frac{3g_s^4}{64 \hat{s}^2}; \quad C_t = \frac{g_s^4}{48(\hat{t} - m_t^2)^2}; \quad r_t = \frac{m_t^2}{\hat{s}}; \quad \beta_t = \sqrt{1 - 4\frac{m_t^2}{\hat{s}}}; \quad g^* = 1. \quad (\text{A30})$$

$$C_u = \frac{g_s^4}{48(\hat{u} - m_t^2)^2}; \quad C_{s\bar{t}} = \frac{3g_s^4}{128\hat{s}(\hat{t} - m_t^2)} \quad (\text{A31})$$

$$C_{su} = \frac{-3g_s^4}{128\hat{s}(\hat{u} - m_t^2)}; \quad C_{tu} = \frac{-g_s^4}{384(\hat{t} - m_t^2)(\hat{u} - m_t^2)} \quad (\text{A32})$$

-
- [1] Tevatron Electroweak Working Group, CDF, and D0 Collaborations, [arXiv:1107.5255](#).
- [2] CDF Collaboration, [Phys. Rev. D **82**, 052002 \(2010\)](#); CDF Collaboration, [Phys. Rev. D **83**, 071102 \(2011\)](#); CDF Collaboration, [Phys. Rev. D **84**, 031101 \(2011\)](#).
- [3] V.M. Abazov *et al.* (D0 Collaboration), [Phys. Rev. D **84**, 012008 \(2011\)](#); V.M. Abazov *et al.* (D0 Collaboration), [Phys. Lett. B **704**, 403 \(2011\)](#).
- [4] N. Kidonakis, [Phys. Rev. D **82**, 114030 \(2010\)](#); [arXiv:1105.3481](#).
- [5] CMS Collaboration, [J. High Energy Phys. **11** \(2012\) 067](#).
- [6] ATLAS Collaboration, [Phys. Lett. B **717**, 89 \(2012\)](#).
- [7] CDF Collaboration, [Phys. Rev. Lett. **101**, 202001 \(2008\)](#).
- [8] V.M. Abazov *et al.* (D0 Collaboration), [Phys. Rev. D **84**, 112005 \(2011\)](#).
- [9] CDF Collaboration, CDF Conference Note 10719.
- [10] V.M. Abazov *et al.* (D0 Collaboration), [Phys. Rev. Lett. **108**, 032004 \(2012\)](#); V.M. Abazov *et al.* (D0 Collaboration), [Phys. Lett. B **702**, 16 \(2011\)](#).
- [11] ATLAS Collaboration, [Phys. Rev. Lett. **108**, 212001 \(2012\)](#).
- [12] CMS Collaboration, CMS Physics Analysis Summary, Report No. CMS-PAS-TOP-12-004.
- [13] ATLAS Collaboration, Atlas Note ATLAS-CONF-2012-133; CMS Collaboration, CMS Physics Analysis Summary, Report No. CMS-PAS-TOP-12-016.
- [14] J. Baglio, M. Beccaria, A. Djouadi, G. Macorini, E. Mirabella, N. Orlando, F.M. Renard, and C. Verzegnassi, [Phys. Lett. B **705**, 212 \(2011\)](#).
- [15] S. Fajfer, J.F. Kamenik, and B. Melic, [J. High Energy Phys. **08** \(2012\) 114](#).
- [16] R.M. Godbole, K. Rao, S.D. Rindani, and R.K. Singh, [J. High Energy Phys. **11** \(2010\) 144](#).
- [17] K. Huitu, S. Kumar Rai, K. Rao, S.D. Rindani, and P. Sharma, [J. High Energy Phys. **04** \(2011\) 026](#).
- [18] S.D. Rindani and P. Sharma, [J. High Energy Phys. **11** \(2011\) 082](#); R.M. Godbole, S.D. Rindani, and R.K. Singh, [Phys. Rev. D **67**, 095009 \(2003\)](#); [Phys. Rev. D **71**, 039902\(E\) \(2005\)](#).
- [19] S.D. Rindani and P. Sharma, [Phys. Lett. B **712**, 413 \(2012\)](#).
- [20] D. Choudhury, R.M. Godbole, S.D. Rindani, and P. Saha, [Phys. Rev. D **84**, 014023 \(2011\)](#); D.-W. Jung, P. Ko, and J.S. Lee, [Phys. Lett. B **701**, 248 \(2011\)](#); J. Cao, K. Hikasa, L. Wang, L. Wu, and J.M. Yang, [Phys. Rev. D **85**, 014025 \(2012\)](#).
- [21] R. Martinez, M.A. Perez, and N. Poveda, [Eur. Phys. J. C **53**, 221 \(2008\)](#).
- [22] J.M. Yang and C.S. Li, [Phys. Rev. D **54**, 4380 \(1996\)](#).
- [23] R. Martinez and J.A. Rodriguez, [Phys. Rev. D **65**, 057301 \(2002\)](#).
- [24] Q.-H. Cao, C.-R. Chen, F. Larios, and C.-P. Yuan, [Phys. Rev. D **79**, 015004 \(2009\)](#); L. Ding and C.-X. Yue, [Commun. Theor. Phys. **50**, 441 \(2008\)](#).
- [25] R. Martinez, M.A. Perez, and O.A. Sampayo, [Int. J. Mod. Phys. A **25**, 1061 \(2010\)](#).
- [26] D. Atwood, A. Kagan, and T.G. Rizzo, [Phys. Rev. D **52**, 6264 \(1995\)](#).
- [27] P. Haberl, O. Nachtmann, and A. Wilch, [Phys. Rev. D **53**, 4875 \(1996\)](#).
- [28] Z. Hioki and K. Ohkuma, [Phys. Rev. D **83**, 114045 \(2011\)](#).
- [29] D. Choudhury and P. Saha, [Pramana **77**, 1079 \(2011\)](#).
- [30] Z. Hioki and K. Ohkuma, [Eur. Phys. J. C **65**, 127 \(2010\)](#); [Phys. Lett. B **71**, 1535 \(2011\)](#).
- [31] H. Hesari and M.M. Najafabadi, [arXiv:1207.0339](#).
- [32] S.K. Gupta and G. Valencia, [Phys. Rev. D **81**, 034013 \(2010\)](#); S.K. Gupta, A.S. Mete, and G. Valencia, [Phys. Rev. D **80**, 034013 \(2009\)](#).
- [33] K.-m. Cheung, [Phys. Rev. D **53**, 3604 \(1996\)](#).
- [34] T.G. Rizzo, [Phys. Rev. D **53**, 6218 \(1996\)](#).

- [35] K.-m. Cheung, *Phys. Rev. D* **55**, 4430 (1997).
- [36] H.-Y. Zhou, *Phys. Rev. D* **58**, 114002 (1998).
- [37] J. L. Hewett and T. G. Rizzo, *Phys. Rev. D* **49**, 319 (1994).
- [38] R. Martinez and J. A. Rodriguez, *Phys. Rev. D* **55**, 3212 (1997); J. F. Kamenik, M. Papucci, and A. Weiler, *Phys. Rev. D* **85**, 071501 (2012).
- [39] R. M. Godbole, S. D. Rindani, and R. K. Singh, *J. High Energy Phys.* **12** (2006) 021; B. Grzadkowski and Z. Hioki, *Phys. Lett. B* **476**, 87 (2000); **529**, 82 (2002); **557**, 55 (2003); Z. Hioki, [arXiv:hep-ph/0210224](https://arxiv.org/abs/hep-ph/0210224).
- [40] J. A. M. Vermaseren, [arXiv:math-ph/0010025](https://arxiv.org/abs/math-ph/0010025).
- [41] J. Pumplin, A. Belyaev, J. Huston, D. Stump, and W. K. Tung, *J. High Energy Phys.* **02** (2006) 032.
- [42] W. Bernreuther, *J. Phys. G* **35**, 083001 (2008).
- [43] C. Englert, A. Freitas, M. Spira, and P. M. Zerwas, *Phys. Lett. B* **721**, 261 (2013).